Science of the Total Environment 865 (2023) 161168

Contents lists available at ScienceDirect

Science of the Total Environment

journal homepage: www.elsevier.com/locate/scitotenv

The iron "redox battery" in sandy sediments: Its impact on organic matter remineralization and phosphorus cycling

Zhe Zhou [a,*], Susann Henkel [a,b], Sabine Kasten [a,b,c], Moritz Holtappels [a,b]

[a] Alfred Wegener Institute Helmholtz Centre for Polar and Marine Research, 27570 Bremerhaven, Germany
[b] Center for Marine Environmental Sciences – MARUM, University of Bremen, 28359 Bremen, Germany
[c] Faculty of Geosciences, University of Bremen, 28359 Bremen, Germany

HIGHLIGHTS

- Aerobic organic matter mineralization is ~12 times faster than anaerobic pathways.
- Reduced Fe is mainly retained in the solid phase as re-oxidizable Fe(II) minerals.
- Solid-phase Fe(III)/Fe(II) can act as a "redox battery" in sands.
- Released P is coprecipitated during aqueous Fe^{2+} re-oxidation ("Fe curtain").
- P released before Fe^{2+} can escape the "Fe curtain" in porewater advection.

GRAPHICAL ABSTRACT

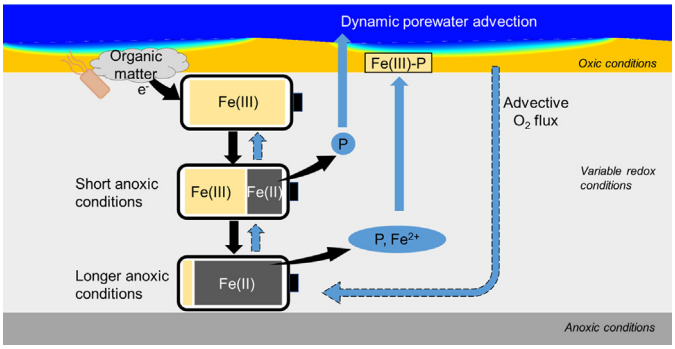

ARTICLE INFO

Editor: Jay Gan

Keywords:
Permeable sediments
Advection
Redox cycling
iron
Organic matter
Phosphorus

ABSTRACT

Permeable sandy sediments cover 50–60 % of the global continental shelf and are important bioreactors that regulate organic matter (OM) turnover and nutrient cycling in the coastal ocean. In sands, the dynamic porewater advection can cause rapid mass transfer and variable redox conditions, thus affecting OM remineralization pathways, as well as the recycling of iron and phosphorus. In this study, North Sea sands were incubated in flow-through reactors (FTRs) to investigate biogeochemical processes under porewater advection and changing redox conditions. We found that the average rate of anaerobic OM remineralization was 12 times lower than the aerobic pathway, and Fe(III) oxyhydroxides were found to be the major electron acceptors during 34 days of anoxic incubation. Reduced Fe accumulated in the solid phase (expressed as Fe(II)) before significant release of Fe^{2+} into the porewater, and most of the reduced Fe (~96 %) remained in the solid phase throughout the anoxic incubation. Fe(II) retained in the solid phase, either through the formation of authigenic Fe(II)-bearing minerals or adsorption, was easily re-oxidized upon exposure to O_2. Excessive P release (apart from OM remineralization) started at the beginning of the anoxic incubation and accelerated after the release of Fe^{2+} with a constant P/Fe^{2+} ratio of 0.26. After 34 days of anoxic incubation, porewater was re-oxygenated and > 99 % of released P was coprecipitated through Fe^{2+} oxidation (so-called "Fe curtain"). Our results demonstrate that Fe(III)/Fe(II) in the solid phase can serve as a relatively immobile and rechargeable "redox battery" under dynamic porewater advection. This Fe "redox battery" is characteristic for permeable sediments and environments with variable redox conditions, making Fe an important player in OM turnover. We also suggest that P liberated before Fe^{2+} release can escape the "Fe curtain" in surface sediments, thus potentially increasing net benthic P efflux from permeable sediments under variable redox conditions.

* Corresponding author.
E-mail address: zhe.zhou@awi.de (Z. Zhou).

http://dx.doi.org/10.1016/j.scitotenv.2022.161168
Received 15 September 2022; Received in revised form 12 December 2022; Accepted 20 December 2022
Available online 23 December 2022

1. Introduction

Permeable sandy sediments cover approximately half of the continental shelves (Hall, 2002). Their high permeability makes advective porewater flow dominate the mass transport and turnover in the surface sediments (Huettel et al., 2014). The dynamic porewater flow facilitates a high efficiency of organic matter (OM) decomposition, making sands not only a biogeochemical filter at the land-sea boundary, but also hot spots for OM remineralization, carbon dioxide release, and nutrient cycling (Cook et al., 2007; Gao et al., 2012).

The pressure gradients driving porewater advection in permeable sands are mainly caused by the interplay of bottom water currents and small-scale sediment topographies, such as ripples. Thus, variable bottom water currents due to waves, tides and residual currents induce variable porewater flow on time scales ranging from seconds to hours to days. Further, bottom water currents induce sediment transport, i.e. the formation and migration of ripples which therefore cause a slow travelling of pressure gradients in the horizontal plane (Precht and Huettel, 2004; Ahmerkamp et al., 2015). In addition, bio-irrigation and bio-turbation caused by benthic infauna can effectively ventilate deeper parts of the sandy sediment (Volkenborn et al., 2010) on time scales depending on the respiratory and migratory behavior of the species. In summary, permeable sands are characterized by a highly variable transport regime in space and time that leads to frequent variations of redox conditions (Ahmerkamp et al., 2017). The constant shift between oxic and anoxic conditions (redox oscillation) affects OM turnover and the cycling of redox-sensitive elements and nutrients (Aller, 1994; Kristiansen et al., 2002; Cook et al., 2007).

During the transition of redox conditions, the main electron acceptors for microbial OM remineralization can shift from O_2 to NO_3^-/NO_2^-, Mn (IV), Fe(III), and SO_4^{2-}. While O_2 and SO_4^{2-} are suggested to represent the main electron acceptors in marine sediments (e.g., Jørgensen and Kasten, 2006; Bowles et al., 2014), the intermediate electron acceptors, such as Fe(III) oxyhydroxides, can also have a significant role in sediment OM remineralization due to their high abundance and repetitive redox cycling (e.g., Canfield et al., 1993; Slomp et al., 1997; Haese, 2006; Wunder et al., 2021; Peiffer et al., 2021). For sands that experience frequent variation of redox conditions in an expanded zone (Ahmerkamp et al., 2017), the contribution of Fe(III) oxyhydroxides to OM remineralization, as well as its role in phosphorus cycling may be of particular importance.

As electron acceptor for OM remineralization, Fe(III) oxyhydroxides are reduced and either released as dissolved Fe^{2+} into the porewater or trapped in the solid-phase as Fe(II) (in the following we use the two expressions to discriminate between reduced iron in dissolved and solid phase). Under porewater advection, Fe^{2+} can be transported away from the Fe-reduction zone much faster than in cohesive sediments where molecular diffusion is limiting the mass transport. Part of the dissolved Fe^{2+} may be advected towards the oxic sediment surface where it is oxidized and precipitates as Fe(III) oxyhydroxide, as shown in flume experiments under stable flow conditions (Huettel et al., 1998). Another fraction of Fe^{2+} may be advected to deeper sulfidic parts of the sediment, where it would form solid iron sulfides (FeS, FeS_2, etc.). The advective transport of dissolved Fe^{2+} and the accumulation of Fe in oxic or sulfidic sediments would rapidly deplete less crystallized, easily reducible Fe(III) in the iron reduction zone. Alternatively, Fe(III) oxyhydroxides can be transformed into secondary Fe (II)-bearing minerals (e.g. $FeCO_3$, FeS_x), which have a distinct potential for re-oxidation (e.g., Canfield, 1989; Kappler et al., 2021). In this case, no reallocation of Fe is involved because there is no change from solid to dissolved phase. Thus, the occurrence of reduced Fe, either as mineral or dissolved ion, strongly affects the repetitive use of Fe as electron acceptor under variable flow and redox conditions. To better evaluate the contribution of Fe to OM remineralization in coastal sands, a closer look into the distribution of reduced Fe and its potential to re-oxidation during redox transitions is needed.

In addition to OM remineralization, Fe redox cycling also plays a crucial role in P retention and recycling during redox transitions both over depth in the sediment and over time (e.g., Slomp et al., 1996; Reed et al., 2011; März et al., 2018; Anschutz et al., 2019). Under anoxic conditions, the sedimentary P retention potential will be diminished, mainly due to the reductive dissolution of Fe(III) oxides, thus leading to the releases of P and Fe^{2+} into the porewater (e.g., Krom and Berner, 1981; Rozan et al., 2002; Küster-Heins et al., 2010; Zhao et al., 2019). Authigenic Fe—P mineral formation (e.g. vivianite) and P adsorption onto secondary minerals can retain part of the liberated P (Kraal et al., 2015; Egger et al., 2015; März et al., 2018). The released P can also be retained by the "Fe curtain" in the oxic layer, where P can be adsorbed or coprecipitated with newly formed Fe oxides, thus preventing excessive P escape into the overlying seawater (Chambers and Odum, 1990; Slomp et al., 1996; Rozan et al., 2002; Gao et al., 2020). In sands, the dynamic porewater flow leaves less time for the adsorption of dissolved P compared to the diffusive transport in cohesive sediments. Coprecipitation during Fe^{2+} oxidation is therefore regarded as the main mechanism to immobilize P in permeable sediments (Kazmierczak et al., 2020). The Fe^{2+}/P ratio in porewater becomes therefore very critical to determine the net P flux from sands. However, detailed understanding and quantification of Fe^{2+} and P release from coastal sands during the transition into reducing conditions are still missing.

Considering the high permeability of sands and the dominant role of advective flow, it is not appropriate to use bottle incubation experiments to quantify the biogeochemical processes mentioned above. For permeable sediments, flow-through-reactors (FTRs) have been used extensively to determine reaction rates under advective flow conditions as previously described by e.g. Rao et al. (2007), Santos et al. (2012) and Ahmerkamp et al. (2020). In this study, we incubated natural North Sea sands in FTRs under recirculating advective flow to simulate the redox transition from oxic to reducing conditions. The biogeochemical processes related to OM remineralization, Fe and P cycling were closely investigated and quantified. Specifically, we tracked the concentrations of dissolved inorganic carbon (DIC), dissolved O_2, pH, NO_3^-, NO_2^-, NH_4^+, P, Fe^{2+}, Mn^{2+}, SO_4^{2-}, and the sum of sulfide species in the circulating porewater over time. The change of element contents in the solid phase was determined using sequential Fe and P extractions and visual microscopic inspection before and after the experiment. To simulate the re-oxidation processes during redox variations, the anoxically incubated sands and porewater were re-oxygenated and the changes in the solid labile Fe and dissolved Fe^{2+}, P, Mn^{2+}, and Si were tracked. The aim of this study was to improve our mechanistic understanding of Fe—P interactions and related fluxes in the highly relevant, but so far understudied sandy sediments.

2. Materials and methods

2.1. Sediment sampling and experimental setup

Sampling was conducted around a subtidal location (55.03° N, 8.46° E, 7–15 m depth) off the island of Sylt, Germany, in August 2020. A Van Veen grab was used to recover sediments, whereby we only collected the upper 1–2 cm of sands with yellowish color. From previous in situ O_2 penetration measurements (e.g. Ahmerkamp et al., 2017), we know that this layer of sediments is mostly oxic with occasional anoxia, thus most likely susceptible to redox oscillations. The collected sands were stored in the dark and covered with seawater until further processing in the AWI laboratories of Sylt on the same day. Natural seawater was also collected at the sampling area and used in this study after filtration over a 0.45 μm filter.

Sands collected from three sites were named based on their average grain size as "fine sand" (186 μm), "medium sand_1" (278 μm) and "medium sand_2" (312 μm) (Table S1). The average grain size of investigated sands encompassed the most abundant types of fine to medium sands (approx. 50 % of the global sand areas). Sands were first sieved with a mesh size of 1 mm to remove large shells and other debris. Afterward, the sands were filled into flow-through reactors (FTRs) as described by Ahmerkamp et al. (2020). Each FTR has an inner diameter of 9 cm and a filled core length of 18 cm, which equals 1145 cm^3 or about 2289 g of dry sand (sediment density ~ 2 g/mL), and about 430 ml porewater (the porosities of three sands were close to 0.4). A plankton net (80 μm mesh)

was placed into the inlet and outlet lid to prevent sediment discharge into the tubing. Tubing with low gas permeability (Fluran™ HCA F-5500-A) was used in this study to limit O_2 diffusion into the porewater. The porewater flow was maintained using a peristaltic pump (ISMATEC REGLO). Further, O_2-optode flow-through cells (OXFTC connected to a 4-channel Firesting O_2 meter, Pyroscience) were mounted in the inflow and outflow tubing to measure the changes in the O_2 concentration at the beginning of the experiment and to monitor potential O_2 intrusion during the anoxic phase.

The FTR incubations were conducted in a dark temperature-controlled room at in-situ temperature of 20 °C (Fig. S1). FTRs filled with sands were first continuously run with air-saturated seawater at a rate of 7 ± 1 mL/min over one day (about 23.4 times of the volume of porewater in FTR per day) until the difference between O_2 concentrations at the inlet and the outlet was constant, indicating a steady uptake of O_2 for aerobic OM remineralization. Afterwards, the outflow and inflow tubings were connected to an air-tight water reservoir to initiate and sustain recirculating flow. The retention time of water in the cores was 1.0 ± 0.2 h. The water reservoir was initially full of air-saturated seawater (610 mL) and was continuously mixed by magnetic stirring. To characterize the changes in the aqueous phase over time, an 8 ml sample from the outflow was collected at each time point. The sampling was conducted while flushing N_2 into the emerging gas phase of the reservoir. Hence, the sample volume was replaced by N_2 in the reservoir. First samples were taken after O_2 at the outlet was nearly depleted (<1.5 μM) to avoid artificial changes in O_2 concentration due to gas-liquid re-equilibration. The sampled solution was divided into different aliquots that were used for immediate analyses and preserved for analysis in the AWI laboratories in Bremerhaven (Germany), respectively. The dilution effect due to the water reservoir and the aqueous volume change due to sampling were considered in all of our calculations. Specifically, the quantity of released species (e.g. Fe^{2+}, DIC, NH_4^+) was calculated by multiplying the measured concentration with the current aqueous volume (after deduction of sampled volume).

In this study, we present the results of a short-term (5 days) and a long-term (34 days) incubation under recirculation mode. For the short-term incubation experiment, we used all three types of sands described above and started the FTR experiments on the day of sediment collection. For the 34 days incubation experiment, we transported the fine sand to the AWI laboratories in Bremerhaven (Germany). To keep the fine sand oxic and close to in situ conditions, it was stored in the dark, with seawater covering and manual mixing from time to time, and used within five days after collection. The fine sands were collected at the same location as the fine sand used in the short-term incubation, but in different batches. Triplicate FTRs filled with fine sand were used for long-term incubation. To characterize the changes in the solid phase, the FTR sediment columns were successively sacrificed after 5, 13, 22, and 34 days in a glovebag filled with N_2. To simulate the reoxygenation, the water reservoir and the incubated sands were re-exposed to air after different periods of the anoxic incubation.

2.2. Porewater analysis

The dissolved oxygen in the in-flow and out-flow was continuously measured with O_2-optode flow-through cells, and calibrated with 0 % and 100 % air-saturated seawater. Dissolved Fe^{2+} was analyzed on-site by directly sampling 1 ml porewater from the outflow into cuvettes pre-filled with 50 μl ferrozine solution, and measured photometrically at 565 nm (Stookey, 1970). The porewater pH was measured immediately in a separate vial with a calibrated portable pH meter. Dissolved inorganic carbon (DIC) samples were stored at 4 °C after poisoning with $HgCl_2$. Nutrient samples (NO_3^-, NO_2^-, NH_4^+, and PO_4^{3-}) were immediately preserved at −20 °C. DIC and nutrient samples were measured with QuAAtro four-channel flow injection Analyzer (Seal Analytical) and respective standard QuAAtro methods (e.g. Q-067-05, Q-084-07). Samples for inductively coupled plasma optical emission spectrometry (ICP-OES, iCAP7000, Thermo Elemental) were acidified with double distilled HCl and stored at 4 °C until measurement. Dissolved P, Si, Mn, and Fe were measured using Yttrium as an internal standard to correct for different ionic strengths of samples. Please note that P measured with ICP-OES was consistent with PO_4^{3-} measurements by the QuAAtro, and we only use the ICP-OES results in this manuscript. Sulfide ($\Sigma H_2S = H_2S + HS^- + S^{2-}$) samples were stabilized with zinc acetate and measured using the methylene blue method (Cline, 1969), but there was no detectable free sulfide in all porewater samples. SO_4^{2-} and Cl^- (1:50 dilution with ultra-pure water) were analyzed by ion chromatography (Metrohm, Compact IC Flex 930). We used the Cl^- concentrations (no significant change expected during incubation) to correct for any variations of SO_4^{2-} due to sampling, treatment, or measurement and calculated the SO_4^{2-} net consumption using Eq. (1) (Weston et al., 2006):

$$\left(SO_4^{2-}\right)_{dep} = \left[\left(Cl^-_{aq}\right)/\left(R_{sw}\right)\right] - {SO_4}^{2-}_{aq} \quad (1)$$

where ${Cl^-}_{aq}$ and ${SO_4}^{2-}_{aq}$ are the measured Cl^- and SO_4^{2-} concentrations in the outflow, and R_{sw} is the molar ratio of Cl^- and SO_4^{2-} of 19.99 measured in the initial seawater used in this study.

2.3. Solid-phase analyses

To determine the grain size distribution, sediments were analyzed with a laser diffraction particle size analyzer (Beckman Coulter, LS 200). Further, sediments were freeze-dried and ground before the measurement of total organic carbon (TOC) with a CNS analyzer (Elementar Vario EL III). To quantify the abundance of labile Fe fractions, as well as their redox state, in the collected sands, we extracted them at the beginning of experiments with 0.5 M HCl in the dark for 1 day (Voelz et al., 2019). After the anoxic incubation, the FTR sediment columns were successively sacrificed at different time points, and solid samples from 5 layers between top and bottom were taken in an anoxic glovebag. Each of those 5 samples was subject to the same 0.5 M HCl extraction. Some additional incubated samples were re-oxygenated by exposure to air over 5 days, and subjected to the same 0.5 M HCl extraction afterwards. A further extraction step with 6 M HCl at 60 °C over 1 day was only applied to the five samples after 34 day incubation. More crystalline Fe(III) oxyhydroxides, such as goethite and hematite, were expected to be extracted (Voelz et al., 2019). The extraction solutions were filtered through a 0.22 μm polyethersulfone membrane filter and measured with an updated ferrozine method to get Fe(II) and the total extracted Fe in samples with low pH (Viollier et al., 2000). Extracted Fe(III) was calculated by subtracting Fe(II) from the total extracted Fe. The potential effects of FeS_x on solid Fe(II) measurements are discussed in the Supplementary Materials. ICP-OES was also applied to measure elements such as Fe, Mn, P, and Si in the extracted solutions. A sequential P extraction was conducted based on Ruttenberg (1992). About 300 mg of sediment was used for the extraction. An in-house reference material (MM91) and extraction blanks were included for quality control. The initial fine sand and those incubated for 13 and 34 days were visually characterized using a stereomicroscope. ^{57}Fe Mössbauer spectroscopy was performed on those samples as well, but was not successful due to the low Fe content and comparably large grain sizes.

3. Results

3.1. Short-term incubation of fine to medium sands

The three sediments used in this study were classified as sand (≥98 %), with average grain sizes in fine sand, medium sand_1, and medium sand_2 ranging from 186 μm to 278 μm and 312 μm, respectively (Table S1). By continuously pumping air-saturated seawater (250 ± 1 μM O_2) through these sands over 1 day, the O_2 concentration in the outflow was stabilized at 133 ± 1 μM in fine sand, 159 ± 1 μM in medium sand_1, and 175 ± 1 μM in medium sand_2, indicating that a steady consumption of O_2 was reached. The setup was then altered to recirculate the porewater in a closed system (Fig. S1). The dissolved O_2 was depleted over 5 h in fine sand, 11 h in medium sand_1, and 16 h in medium sand_2 (Fig. 1.a). To allow the comparison between changes in porewater and solid phase, we normalized all

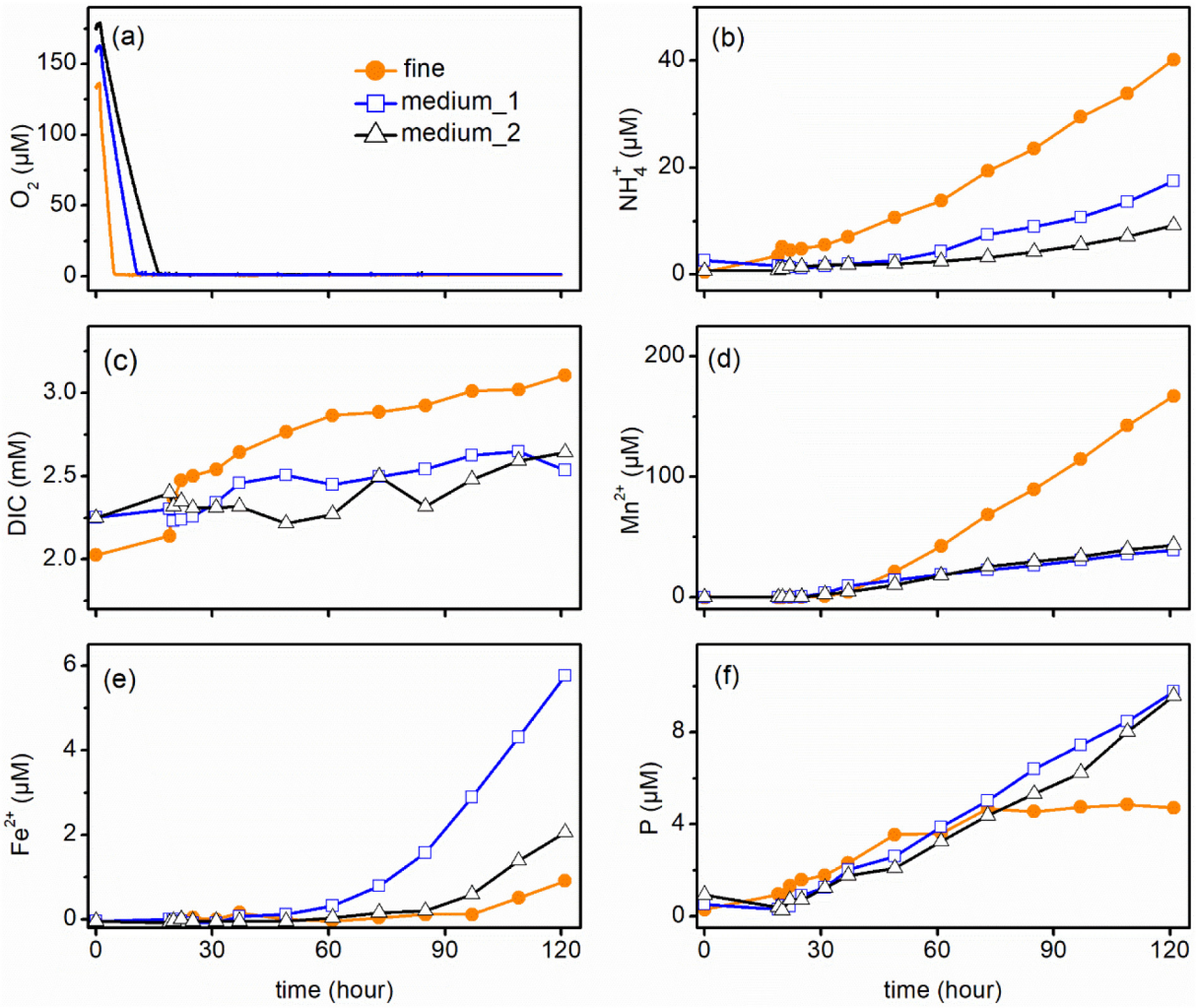

Fig. 1. The concentrations of (a) O_2, (b) NH_4^+, (c) DIC, (d) Mn^{2+}, (e) Fe^{2+}, and (f) P in the outflow of FTRs filled with different sands over 5 days incubation under recirculation mode.

concentrations to per liter of bulk (wet) sands. Oxygen consumption rates per liter sand during incubation under recirculation mode were 58.0 μmol/h in fine sand, 31.5 μmol/h in medium sand_1, and 23.8 μmol/h in medium sand_2. After depletion, dissolved O_2 in all FTRs remained under the sensor's detection limit (0.3 μM) over the following days, showing that the systems were well maintained under anoxic conditions.

NO_3^- was rapidly depleted in the fine sand within 9.5 h, whereas it took 16 h in medium sand_1 and 22 h in medium sand_2 (data not shown). NH_4^+ in the fine sand increased linearly, with 0.34 μmol/h produced per liter sand, much faster compared to 0.11 μmol/h in medium sand_1 and 0.065 μmol/h in medium sand_2 (Fig. 1.b). As another indicator for OM remineralization, DIC concentrations in fine sand rapidly increased in the first two days, followed by a slower and steady increase. The trend of increasing DIC concentrations was less pronounced in the two medium sands (Fig. 1.c).

The release of Mn from the fine sand occurred earlier and at a higher rate than from the two medium sand columns (Fig. 1.d). In contrast, the start of Fe^{2+} release was later in the fine sand (~4.5 days) where more labile Fe was extracted by 0.5 M HCl (Table 1). After 5 days of anoxic incubation, the amount of Fe^{2+} released into the circulating porewater was very limited (<6 μM) in all sands (Fig. 1.e). However, in the solid phase, 3.8 and 2.8 mmol Fe(II) per liter sand were extracted from fine sand and medium sands with 0.5 M HCl at this time point (Table 1), showing that extensive net Fe reduction occurred before Fe^{2+} was measured in the circulating porewater, and most of the reduced Fe remained in the solid.

Based on the sequential P extraction, Fe-bound P (extracted with citrate-dithionite-bicarbonate) accounted for 33–53 % of the total P in the initial sands (Table 1), showing the importance of the Fe sink for P immobilization/storage under oxic conditions. During the incubation under the recirculation mode, dissolved P in the porewater steadily increased over time (Fig. 1.f). The ratio of released NH_4^+/P after 5 days was 9.3 in fine sand, 1.9 in medium sand_1, and 0.97 in medium sand_2, respectively. These values are all lower than the Redfield ratio (16:1).

3.2. Long-term incubation of fine sand

Fine sand was first incubated with a constant air-saturated seawater flow (250 ± 1 μM O_2), and the O_2 concentration in the outflow reached a constant value of 92 ± 10 μM overnight, slightly lower than we observed in short-term incubation experiments. Based on the O_2 consumption measured here, we estimated the rate of aerobic OM remineralization in fine sand to be about 1.07 mmol C (L sediment)$^{-1}$ d^{-1}. After switching into recirculation mode, the dissolved O_2 was depleted after 4 h and the sands were incubated at anoxic conditions over 34 days (Fig. 2.a). NO_3^- was also rapidly depleted within 9 h (i.e. between first and second sampling point), while NH_4^+ accumulated due to the anaerobic decomposition of OM (Fig. 2.b). It is interesting to note that NO_2^- emerged at 5 days and steadily increased to 2.2 μM.

After the depletion of O_2 and NO_3^-, the Mn concentration increased and reached the plateau value of 304 ± 18 μM at 11 days (Fig. 2.c.). Before Mn

Table 1
Results of solid-phase extractions and characterization of sands with different incubation times.

Sands	Time (d)	0.5 M HCl extraction[a]				6 M HCl extraction (μmol Fe/g sand)	TOC		P sequential extraction		
		μmol Fe(II) /g sand	mmol Fe(II) / L sediment	μmol Fe/g sand	Fe(II) /Fe_{tot}		% weight	mmol OC / L sediment	$P_{Fe\text{-}bound}$[b] (μmol/g sand)	P_{tot}[c] (μmol/g sand)	$P_{Fe\text{-}bound}$ / P_{tot}
Fine	0	<DL	<DL	13.20	0	–	0.057 ± 0.004	73.53 ± 5.16	0.77	2.32	0.33
	5	2.47 ± 0.12	3.82 ± 0.19	13.23 ± 1.48	0.19	–	0.059 ± 0.003	76.11 ± 3.87	0.70	1.82	0.39
medium_1	0	<DL	<DL	8.13	0	–	0.049 ± 0.003	63.21 ± 3.87	0.60	1.25	0.48
	5	1.79 ± 0.16	2.77 ± 0.25	8.88 ± 1.0	0.20	–	0.044 ± 0.001	56.76 ± 1.29	0.62	1.65	0.38
medium_2	0	<DL	<DL	8.11	0	–	0.047 ± 0.007	60.63 ± 9.03	0.91	1.72	0.53
	5	1.81 ± 0.15	2.80 ± 0.23	8.71 ± 0.38	0.21	–	0.047 ± 0.003	60.63 ± 3.87	0.97	2.36	0.41
Fine[d]	0	<DL	<DL	11.94 ± 0.36	0	19.34 ± 1.86	0.062 ± 0.005	79.97 ± 6.45	0.76	2.11	0.36
	13	4.10 ± 1.07	6.33 ± 1.65	11.92 ± 0.86	0.40	18.70 ± 0.54	0.058 ± 0.001	74.82 ± 1.29	–	–	–
	22	4.79 ± 0.61	7.40 ± 0.94	11.66 ± 0.50	0.41	18.87 ± 0.73	0.054 ± 0.001	69.66 ± 1.29	–	–	–
	34	5.68 ± 0.59	8.77 ± 0.91	11.08 ± 0.48	0.52	15.01 ± 1.55	0.049 ± 0.002	63.21 ± 2.58	0.70	1.79	0.39

[a] Five samples from each sacrificed (incubated) reactor were measured and reported as average ± standard deviation; <DL means below detection limit of ferrozine method for Fe^{2+} concentration (0.3 μM).
[b] Extraction with citrate-dithionite-bicarbonate.
[c] Total P extracted using the method present by Ruttenberg, 1992.
[d] Sands were collected from the same location as fine sands mentioned above, but in different batches and incubated in different laboratories.

reached the plateau, Fe^{2+} release started and linearly increased to 410 ± 57 μM at day 20 and stabilized thereafter. It was at the same time point when a steady trend of net sulfate consumption was established (Fig. 2.e). Sulfide was not detected in any of the samples taken throughout the anoxic incubation. A continuous release of P and Si was observed during the anoxic incubation (Fig. 2.d).

Based on the 0.5 M HCl extraction of the solid phase, we found that most of the reduced Fe(II) remained in the solid phase, and the amount of solid Fe (II) kept increasing over the incubation even after no further aqueous Fe^{2+} increase was observed (Table 1, Fig. 3). The color change of sand over the anoxic incubation was recorded under a stereomicroscope (Fig. S2). The yellowish coatings in the initial sand were diminished over the time of the incubation, whereas some blackish coatings were formed between day 22 and day 34, coinciding with the increase of net SO_4^{2-} consumption.

To evaluate the rate of OM remineralization, we also monitored DIC over the 34 days of anoxic incubation. We observed a steady increase in

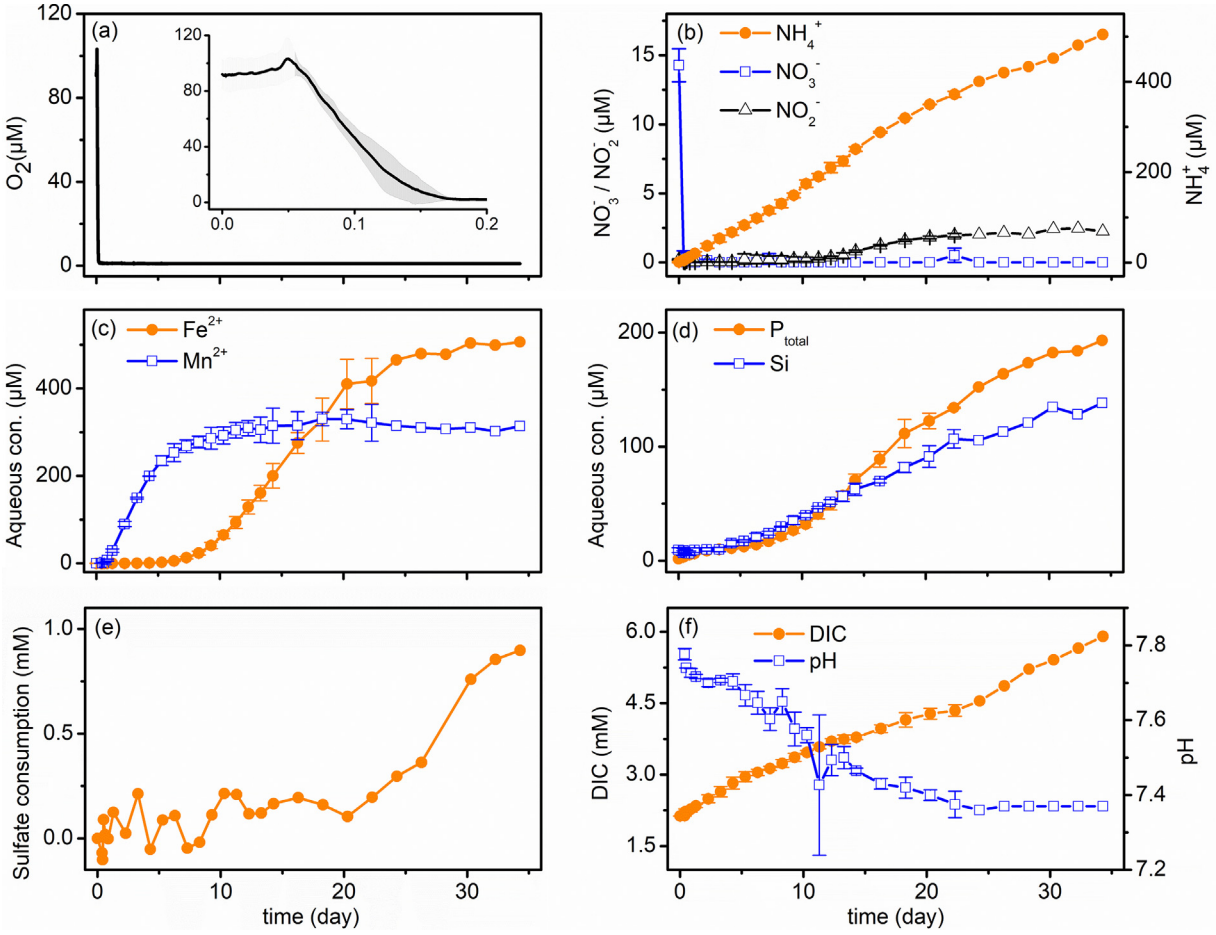

Fig. 2. The concentrations of various parameters in the outflow of the FTRs filled with fine sand over 34 days incubation under recirculation mode. (a) Dissolved O_2 with an inset figure of the first 0.2 day; (b) NO_3^-, NO_2^-, and NH_4^+; (c) Mn^{2+} and Fe^{2+}; (d) P and Si; (e) SO_4^{2-} net consumption (f) DIC and pH;. Data points represent the mean value in triplicate FTRs. Detailed results from each FTR can be found on PANGAEA with same title under open access.

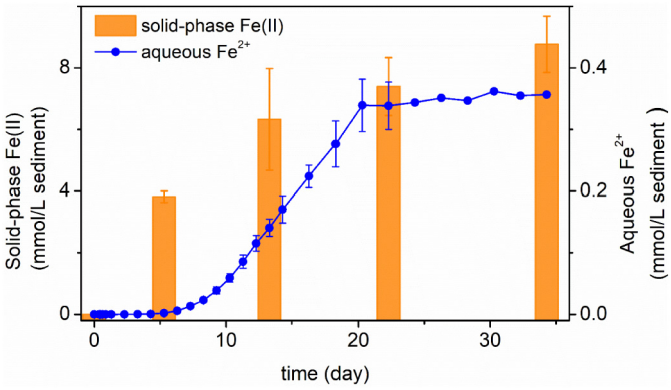

Fig. 3. The distribution of reduced Fe over 34 days incubation under recirculation mode. To make it comparable between solid and aqueous phases, we used the unit of mmol Fe / L sediment here. Please note that the solid-phase Fe(II) data at day 5 was based on the results of short-term incubation.

DIC accompanied by a decrease in pH (Fig. 2.f). Based on the DIC increase and the changes of main electron acceptors, we estimated the average rate of anaerobic OM remineralization as 0.09 ± 0.03 mmolC· (L sediment)$^{-1}$ d^{-1}. By cross-plotting the amount of DIC and NH_4^+ released over time, we found a general fit with the Redfield ratio of C/N (6.6) (Fig. 4.a). The TOC content in the fine sands gradually decreased over the anoxic incubation (Table 1). Due to the low TOC contents in the sands (0.047–0.062 % weight) and the limitation of measurement precision, we only used the TOC data for qualitative analysis.

As depicted in Fig. 4.b, the release of P started earlier than that of Fe^{2+}. With increasing Fe^{2+}, there was a linear correlation between porewater P and Fe^{2+} with a ratio of 0.26. When net sulfate consumption rapidly increased after 22 days, there was no further significant Fe^{2+} release, while P release continued (Figs. 2 and 4.b). The P/NH_4^+ ratio increased significantly after the release of Fe^{2+} (Fig. 4.c); it resulted to be much higher than the Redfield ratio of P/N (1:16). When focusing at the beginning of the anoxic incubation (Fig. 4.d), the ratio of P/ NH_4^+ was also high in the first 2.3 days, followed by a period (2.3 to 6.3 days) in which the ratio was close to the Redfield ratio.

We further evaluated the contributions of the different electron acceptors for OM mineralization over the incubation under recirculation mode. Based on the observed changes of the main electron acceptors, there was about 1.8 times more organic carbon oxidized than reflected in the released DIC (Fig. 5). Fe(III) oxyhydroxides represented the main electron acceptors over 22 days of the anoxic incubation, and most of their contribution was related to changes in the solid phase (Fig. 5). The contribution of SO_4^{2-} rapidly increased between day 22 and 34. Please note that FeS formed during SO_4^{2-} reduction might also be extracted by 0.5 M HCl. But at least in the first 22 days of incubation, the respective amount of FeS (estimated based on the net SO_4^{2-} consumption) and the potential error it may cause in

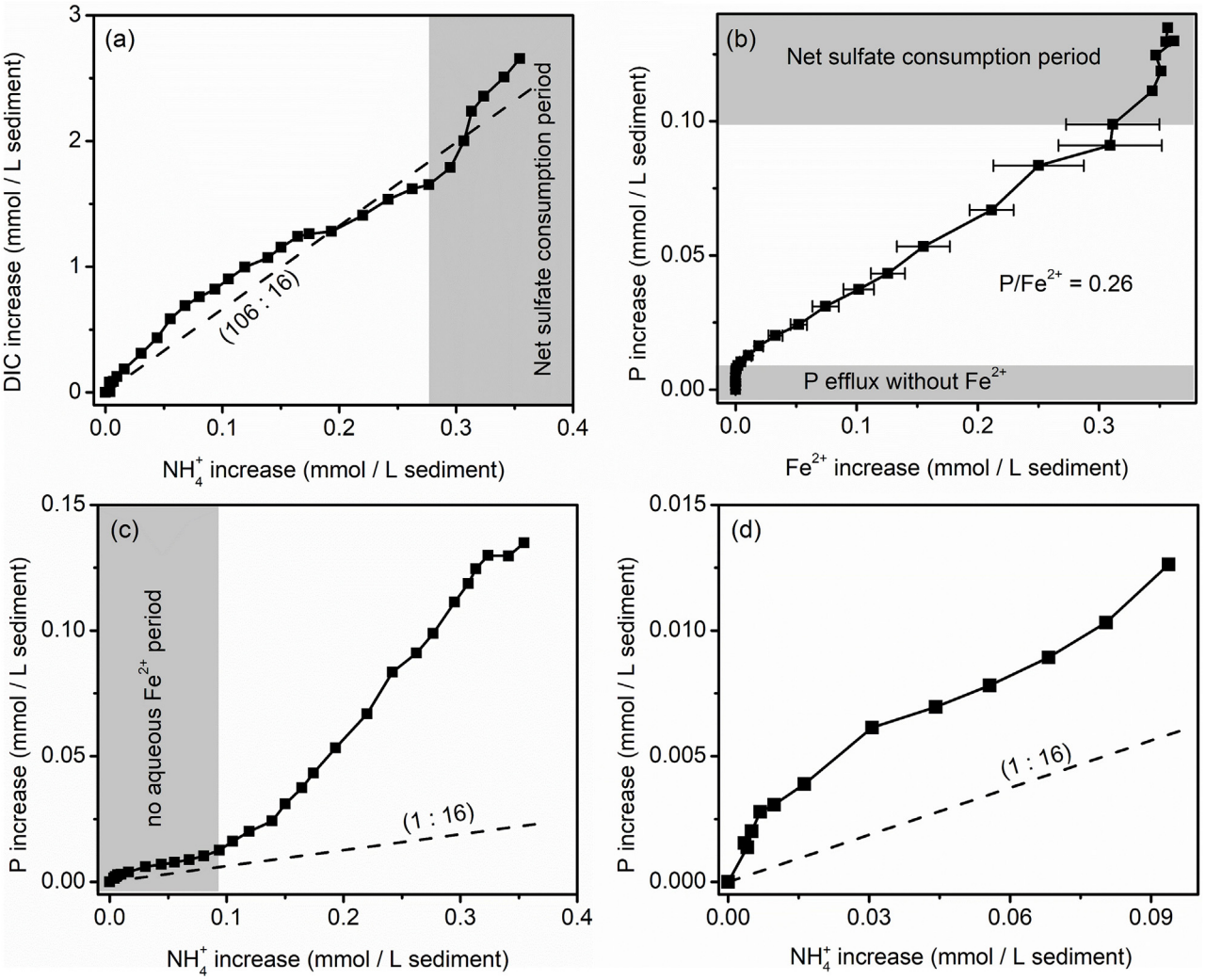

Fig. 4. Cross-plot of the progressive increases (in mmol/ L sediment) of (a) DIC / NH_4^+, (b) P / Fe^{2+}, (c) P / NH_4^+, and (d) P / NH_4^+ within the no aqueous Fe^{2+} period. The dashed lines shown in (a), (b), and (c) represent the Redfield ratio of C/N and P/N.

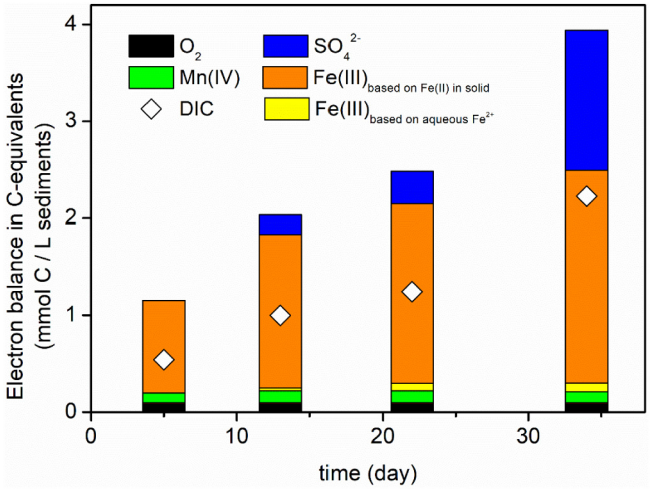

Fig. 5. The estimated contribution of major electron acceptors (expressed in C-equivalents) to OM remineralization, and the measured DIC release at different days of incubation under recirculation mode. Please note that the Fe(III) contribution can be overestimated after net sulfate consumption started as the released sulfide might also reduce Fe(III), but it was quantitatively not significant in the first 22 days. NO_3^- was not added due to negligible share in this experiment.

0.5 M HCl extraction (excessive Fe(III) reduction by released sulfide) is <5 % of the measured Fe(II) (for details see Supplementary Material).

3.3. Re-oxidation of porewater and sands

To simulate redox oscillation as typically occurring in permeable surface sediments, we re-oxygenated the water in the reservoir and the sands after the anoxic incubation. As O_2 concentrations increased in the water, we first observed the formation of white flocs in the solution before any Fe^{2+} oxidation was detected (Fig. S3). At O_2 concentrations of ~78 μM, Fe^{2+} was no longer detected in the reservoir, and all Fe^{2+} was oxidized and precipitated. At the same time, we measured that >99 % of dissolved P was removed, while 85 % of Si and 94 % of Mn remained in the aqueous phase (Fig. 6). Please note that 96 % of Al, 86 % of As, and 42 % of Ba were also removed from the solution during re-oxidation (data not shown). Solid Fe(II) (extracted with 0.5 M HCl) was absent in the incubated sands after 5 days of re-oxidation.

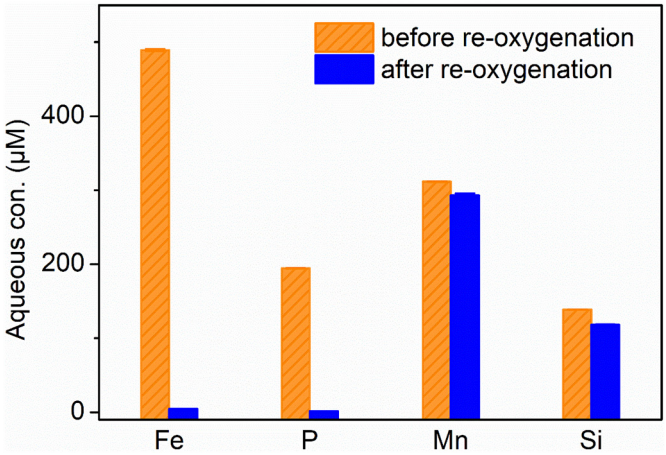

Fig. 6. The dissolved Fe, P, Mn, and Si in the circulated porewater (after 34 days of anoxic incubation) before and after reoxygenation.

4. Discussion

4.1. Rates of organic matter remineralization in sands

The rates of OM remineralization, as indicated by O_2 consumption during oxic conditions and the production of DIC and NH_4^+ during anoxic conditions, were both higher in the sand with smaller mean grain size (Fig. 1). In fine sand, the TOC content was higher than in the medium sands (Table 1), and the absolute amount of labile OM is expected to be also higher (Keil et al., 1994). In addition, we identified a higher abundance of labile Fe and Mn oxides in finer sands that could serve as electron acceptors for anaerobic OM remineralization (Table 1, Fig. 1.d). Furthermore, fine sands are known to offer a larger surface area available for microbial colonization compared to medium-sized sands, resulting in increased cell numbers and respiration rates per volume (Ahmerkamp et al., 2020). All of these factors are likely to have contributed to the observed higher rates of microbial OM remineralization in the FTR column filled with fine sand.

Based on the O_2 consumption during pumping air-saturated seawater through fine sand, we determined an aerobic OM remineralization rate of 1.07 ± 0.12 mmol C· (L sediment)$^{-1}$·d^{-1}. This was about 12 times faster than the anaerobic OM remineralization (0.09 ± 0.03 mmol·C (L sediment)$^{-1}$· d^{-1}) estimated based on 34 days of anoxic incubation. Our results are similar to a previous study of fine sands (from False Bay, US), using a thin-layer incubation technique (Kristensen et al., 1995), in which the authors reported that aerobic OM remineralization was ~10 times faster than under anoxic conditions. Higher rate of OM remineralization under oxic conditions compared to anoxic conditions is well known (e.g. Canfield et al., 1993; Aller, 1994; Jørgensen, 2006), and the importance of aerobic OM turnover in coastal sands is more significant than in coastal cohesive sediments (Werner et al., 2006; Huettel et al., 2014). The extent of the oxic zone in coastal cohesive sediments is in the range of a few hundred micrometers to millimeters (Jørgensen, 2006) and can be temporally expanded through bioturbation and bioirrigation (Aller, 1994). The oxygen penetration depth in permeable sands is in the range of millimeters to centimeters, favoring aerobic OM remineralization in a broader zone (Precht et al., 2004; Ahmerkamp et al., 2017). The high efficiency of aerobic OM remineralization in the expanded oxic zone accelerates the overall OM remineralization rate and reduces OM burial efficiency in sands (de Beer et al., 2005; Rusch et al., 2006), which is consistent with the observed low TOC contents in the sands used in our experiments (Table 1). The study area was estimated to have high OM input from primary productivity (~309 g·C·m^{-2}·y^{-1}) and terrestrial sources (~110 g·C·m^{-2}·y^{-1}), and 10–20 % of the remineralization may occur in the sediments (van Beusekom et al., 1999). Coastal sands therefore can function as efficient sites for OM degradation and CO_2 emission, and play a crucial role in carbon cycling in the coastal ocean.

4.2. Iron as electron acceptor in sands

The significant role of microbial Fe(III) reduction in OM degradation has been suggested by many researchers (e.g., Canfield et al., 1993; Van Cappellen and Wang, 1996; Wunder et al., 2021; Baloza et al., 2022). Here we focused on the less crystallized, easily reducible Fe(III) (extracted with 0.5 M HCl) and explored its role as electron acceptor under advective flow in coastal sands characterized by variable redox conditions.

In the initial fine sand, the fraction of 0.5 M HCl extractable Fe(III) makes up 38 % of the total amount of extractable Fe(III) oxyhydroxides (by 0.5 M and 6 M HCl, Table 1), suggesting a low crystallinity and possibly high bioavailability of Fe(III) oxyhydroxides. Over 34 days of incubation under recirculation mode, Fe(III) oxyhydroxides were found to serve as the main electron acceptors during the transition of redox conditions (Fig. 5), and most of the reduced Fe(II) (~96 %) was retained in the solid phase (Fig. 3). It was shown that reduced Fe(II) can be trapped in the solid phase either through adsorption to grain surfaces or precipitation of authigenic Fe(II)-bearing minerals (e.g. Fe sulfides, siderite, vivianite) (e.g., Coleman et al., 1993; Thamdrup et al., 1994; Kasten et al., 1998;

Riedinger et al., 2005, 2017; Gorski and Scherer, 2011; März et al., 2018; Kamran et al., 2020).

In marine sediments, the formation of authigenic Fe sulfide minerals is generally regarded as the most important process to retain Fe(II) in the solid phase (e.g., Coleman et al., 1993; Thamdrup et al., 1994; Kasten et al., 1998; Riedinger et al., 2005, 2017). Sulfide formed through sulfate reduction can be re-oxidized to sulfate using Fe(III) as the terminal electron acceptor (the cryptic S cycling) (e.g. Riedinger et al., 2010; Michaud et al., 2020), or precipitate with Fe^{2+} to form blackish Fe sulfides resulting in net sulfate consumption (e.g., Rickard and Luther, 2007; Riedinger et al., 2017). Cryptic S cycling cannot be shown in this study, but the formation of Fe sulfides is consistent with our observations between day 22 and day 34, when net sulfate consumption increased, but there was no detectable sulfide and no further Fe^{2+} release in the porewater (Fig. 2.c). At the same time, Fe(II) in the solid phase increased (Table 1), coincident with the formation of blackish precipitates (e.g. mackinawite) (Fig. S2). We note that the net sulfate consumption caused by the formation of authigenic Fe sulfide minerals can lead to an overestimate of the contribution of Fe reduction to the OM remineralization. This may also partially explain the observed imbalance between DIC and electron acceptors (Fig. 5).

The net sulfate consumption, however, was only about 0.17 mmol / L sediment before day 22 (Fig. 2.e), suggesting that the formation of Fe sulfides is not the main mechanism to retain Fe(II) in the solid phase (~7.4 mmol / L sediment) during the first 22 days of the anoxic incubation. Therefore, we speculate that microbial Fe(III) reduction and promoted carbonate precipitation (e.g. siderite) contribute to retaining Fe(II) in the solid phase during the early period of anoxic incubation, and delay the release of Fe^{2+} into porewater. Previous studies showed that microenvironments could be formed around the surface of microbes, with modified local pH, ion concentrations/activities, and crystal nucleation sites, promoting mineral precipitates even without an oversaturation of ions in the bulk porewater (Coleman et al., 1993; Zeng and Tice, 2014; Hoffmann et al., 2021). The promoted Fe carbonate precipitation (e.g. siderite) is consistent with our observation of the imbalance between DIC and estimated OM oxidation based on electron acceptor consumptions (Fig. 5). As part of carbonate produced from OM remineralization was precipitated with Fe(II), the release of DIC and Fe^{2+} were both impeded. This speculation may look contradictory to the ratio of DIC/NH_4^+ in the porewater, which is close to the Redfield ratio (Fig. 4.a). However, it should be noted that the C/N ratio of OM in surface sandy sediments can be much higher than the Redfield ratio, amongst others the abundance of carbohydrate was reported nearly 10 times than that of amino acids (Fabiano et al., 1995). We also calculated the saturation state of the porewater with respect to vivianite and siderite at day 22, showing that the direct precipitation of these Fe(II)-bearing minerals from porewater could contribute to retaining Fe(II) in the solid phase.

Our observation of impeded Fe^{2+} release as a consequence of the formation of authigenic Fe(II)-bearing minerals (e.g. Fe sulfides, siderite) implies that the labile Fe phase in sands has limited mobility under in situ conditions. Most of the reduced Fe is stationary and won't be flushed away via porewater advection, which otherwise would diminish the labile Fe in the zone with frequent redox oscillation. In addition, our results show that the authigenic Fe(II) minerals in the solid phase were rapidly re-oxidized, making Fe available again as electron acceptor. Based on these results, we suggest that the cycling of Fe(III)/Fe(II) in the solid phase of sands functions as an immobile and rechargeable "redox battery", which can be repetitively used for OM remineralization under frequent redox oscillation.

This Fe "redox battery" has broader implications for coastal sands than for cohesive sediments. In contrast to cohesive sediments where diffusion-dominated diagenesis often produces layered and mostly horizontally arranged redox zones (e.g. Canfield et al., 1993; Kasten et al., 1998; Henkel et al., 2018), sands have a more complex three-dimensional geochemical zonation generated by variable advective porewater flow, and experience much more frequent redox oscillation in an expanded zone (Huettel et al., 1998; Precht et al., 2004). Therefore, the Fe "redox battery" can be used more frequently and in a wider zone in sands compared to cohesive sediments, where redox oscillations in surface sediments are mainly caused by occasional bioturbation and bioirrigation (e.g. Haese, 2006; Van De Velde and Meysman, 2016). With the dynamic advective flow as well as the faunal activities, the occasional O_2 flux into sands oxidizes Fe(II) in the solid phase, at the same time reducing the direct contribution of O_2 for OM remineralization. The authigenic Fe(III) oxyhydroxides produced by re-oxidation in turn have increased importance for the decomposition of OM in the following anoxic phase. These effects and contributions of the Fe "redox battery" are not apparent in porewater profiles and its dynamic is easily overlooked in solid phase profiles. We highlight the importance of the Fe "redox battery" when interpreting field data or setting up biogeochemical models, especially for permeable sediments.

4.3. The impact of iron on phosphorus cycling

Fe(III) oxyhydroxides were shown to function as an important sink for P under oxic conditions and can turn into a source of P under anoxic conditions, thus playing a significant role in the benthic cycling of P (e.g., Slomp et al., 1996; Filippelli and Delaney, 1996; Dellwig et al., 2010; Küster-Heins et al., 2010). In our study, we found that >30 % of the total P in the original coastal sands was bound to Fe (Table 1). During the anoxic incubation, a continuous release of P was observed. The higher ratio of released P/NH_4^+ compared to the Redfield ratio (1:16) suggested the release of P in excess of OM remineralization. This excessive P release was observed even before the extensive net Fe^{2+} release (Fig. 1b + f, Fig. 4b + c). It supports our finding that authigenic Fe(II) minerals that have less affinity to P start to precipitate during the early phase of the anoxic incubation. During further reducing conditions, the central role of organoclastic Fe reduction in the excessive P release was clearly shown by the linear correlation of released P/Fe^{2+} between day 4 and day 22 (Fig. 4d), followed by P release most likely driven by sulfide-induced Fe (III) reduction (e.g. März et al., 2008; Wu et al., 2019; Zhao et al., 2019).

Detailed insights into the interplay of Fe mineralogy and P distribution during Fe(III) reduction were given by previous studies (e.g. Roden and Edmonds, 1997; Küster-Heins et al., 2010; Kraal et al., 2015; März et al., 2018). Generally, microbial reduction and transformation of Fe(III) oxyhydroxides reduces the surface area available for phosphorus adsorption and causes the release of P and Fe^{2+} (e.g. Jensen et al., 1995; Küster-Heins et al., 2010). However, some secondary Fe(II)-bearing minerals (e.g. siderite, magnetite, green rust) that form under anoxic but non-sulfidic conditions can still absorb P, thus impeding the release of Fe^{2+} and P (Roden and Edmonds, 1997; Kraal et al., 2015). In addition, high concentrations of Fe^{2+} and PO_4^{3-} may induce the formation of authigenic Fe (II) phosphates (e.g. vivianite) (Dellwig et al., 2010; März et al., 2018), which could also happen in our long-term anoxic incubation (over saturation for vivianite precipitation). These mechanisms alleviated P release and retained a big fraction of Fe(III)-bound P in the solid phase under anoxic conditions. However, we note that if the anoxic incubation lasts even longer and the FTR columns are transferred into more sulfidic conditions, FeS_x minerals that have minimal affinity for P will replace the reactive Fe mineral pool, and induce the further release of P into the porewater (März et al., 2008; Reed et al., 2011; Pan et al., 2019).

Our study also shows the important role of Fe in benthic P cycling during the transition from anoxic to oxic conditions. As more Fe(III)-bound P was released with longer anoxic incubation, more Fe^{2+} was also accumulated in porewater. After re-oxygenating the porewater in the reservoir incubated for 34 days, nearly all released P (>99 %) was retained, mainly via Fe^{2+} re-oxidation and coprecipitation ("Fe curtain") (Fig. 6). Due to advective porewater flow and decreased adsorption time for P flux in the oxic layer, the "Fe curtain" becomes a major barrier to net P efflux in sands (e.g. Rozan et al., 2002; Smith et al., 2011; Kazmierczak et al., 2020). The net Fe^{2+} release under anoxic conditions, however, can be delayed with authigenic Fe(II) mineral formation that traps reduced Fe in the solid phase. Although a limited amount of P (~0.013 mmol/L sediments) was liberated before Fe^{2+} release (Fig. 4.d), it is still higher than P left in the aqueous phase (~0.001 mmol/L sediments) after reoxygenation of FTR columns incubated over 34 days. Therefore, we hypothesize that the particular

geochemical conditions as found in the early stage of transition into anoxic conditions, allow for P to escape the "Fe curtain" as long as Fe^{2+} is not yet released into the porewater. Thus, the frequency of redox oscillation and the duration of anoxic conditions may affect net benthic P efflux from sands. We further hypothesize that variable redox conditions can generally increase the mobility of Fe(III)-bound P, thus increasing the net benthic P efflux from coastal surface sediments. The compromised "Fe curtain" in permeable sediments, either due to reduced adsorption time under advective flow or impeded Fe^{2+} release under frequent redox oscillation, makes Fe phases less efficient to control the benthic P efflux into the water column. Such an increase in P efflux from permeable sediments can affect primary production in the water column, especially in regions with severe P limitation as recently reported for the nearshore North Sea (e.g., Burson et al., 2016).

5. Conclusions

This study focused on the role of Fe in OM remineralization and P cycling in coastal permeable sediments that are characterized by advective flow and variable redox conditions. Our results show the dominant contribution of Fe(III) oxyhydroxides as electron acceptor for anaerobic OM remineralization during the redox oscillations. Importantly, we found that net Fe^{2+} release was delayed during anoxic incubation under advective flow, and most of the reduced Fe remained in the solid phase as easily re-oxidizable authigenic Fe(II) minerals. Therefore, we suggest that solid-phase Fe(III)/Fe(II) can serve as an immobile and rechargeable "redox battery".

Our results also demonstrate the strong correlation of Fe and P during redox transitions in permeable sediments. Interestingly, we found that the impeded Fe^{2+} release may facilitate P to escape from Fe^{2+} oxidation and co-precipitation ("Fe curtain") under oxic conditions, thus potentially increasing the net advective P efflux from permeable sediments. Therefore, we suggest that the frequency of redox oscillation, which is affected by tide and wave-driven hydrodynamics as well as by sediment morphodynamics, can play an important role in benthic P cycling, and further affect nutrient stoichiometry (e.g. N/P ratio) in the water column.

Our results qualitatively reflect the processes in the field and are realistic for low-frequency redox oscillation in the order of hours to days (e.g. caused by ripple migration). The performance of the iron "redox battery" and P cycling under more frequent redox oscillation are still need further investigation. However, we speculate that high frequency redox oscillation and more erratic conditions as found in situ may further increase the importance of iron in OM remineralization and P cycling.

CRediT authorship contribution statement

Zhe Zhou: Conceptualization; Investigation; Data curation; Writing.
Susann Henkel: Investigation; Writing.
Sabine Kasten: Writing; Funding acquisition; Project administration.
Moritz Holtappels: Conceptualization; Investigation; Writing; Funding acquisition.

Data availability

Data will be made available on request.

Declaration of competing interest

The Authors declare that there is no conflict of interest.

Acknowledgments

The authors would like to thank I. Dohrmann, I. Stimac, and V. Schumacher for their assistance in field trip preparation and sample analysis. We thank the crew of the research vessel *Mya-II* as well as the staff members of AWI's facilities on Sylt. We thank Finn Mielck for the grain size analysis at AWI Sylt. Special thanks go to Dr. Gonzalo Gomez for joining the campaign and the many hours he helped during this study. We also want to thank Professor A. Kappler and Dr. P. Joshi from the University of Tübingen for their help with Mössbauer spectroscopy measurement. We would like to thank the three reviewers whose comments greatly improved this work. This work was funded by the AWI INSPIRES I program under the framework of Helmholtz Research Program "Changing Earth - Sustaining our Future" (PoF IV) and by the Deutsche Forschungsgemeinschaft through the Cluster of Excellence "The Ocean Floor—Earth's Uncharted Interface" (Germany's Excellence Strategy—EXC-2077). We acknowledge support by the Open Access Publication Funds of Alfred-Wegener-Institut Helmholtz-Zentrum für Polar- und Meeresforschung

Appendix A. Supplementary data

Supplementary data to this article can be found online at https://doi.org/10.1016/j.scitotenv.2022.161168.

References

Ahmerkamp, S., Winter, C., Janssen, F., Kuypers, M.M., Holtappels, M., 2015. The impact of bedform migration on benthic oxygen fluxes. J.Geophys.Res.Biogeosci. 120, 2229–2242.
Ahmerkamp, S., Winter, C., Krämer, K., Beer, D.d., Janssen, F., Friedrich, J., Kuypers, M.M., Holtappels, M., 2017. Regulation of benthic oxygen fluxes in permeable sediments of the coastal ocean. Limnol. Oceanogr. 62, 1935–1954.
Ahmerkamp, S., Marchant, H.K., Peng, C., Probandt, D., Littmann, S., Kuypers, M.M.M., Holtappels, M., 2020. The effect of sediment grain properties and porewater flow on microbial abundance and respiration in permeable sediments. Sci. Rep. 10, 3573.
Aller, R.C., 1994. Bioturbation and remineralization of sedimentary organic matter: effects of redox oscillation. Chem. Geol. 114, 331–345.
Anschutz, P., Bouchet, S., Abril, G., Bridou, R., Tessier, E., Amouroux, D., 2019. In vitro simulation of oscillatory redox conditions in intertidal sediments: N, Mn, Fe, and P coupling. Cont. Shelf Res. 177, 33–41.
Baloza, M., Henkel, S., Geibert, W., Kasten, S., Holtappels, M., 2022. Benthic carbon remineralization and iron cycling in relation to sea ice cover along the eastern continental shelf of the Antarctic Peninsula. J.Geophys.Res.Oceans 127, e2021JC018401.
de Beer, D., Wenzhöfer, F., Ferdelman, T.G., Boehme, S.E., Huettel, M., van Beusekom, J.E., Böttcher, M.E., Musat, N., Dubilier, N., 2005. Transport and mineralization rates in North Sea sandy intertidal sediments, Sylt-Rømø basin, Wadden Sea. Limnol. Oceanogr. 50, 113–127.
van Beusekom, J.E.E., Brockmann, U.H., Hesse, K.J., Hickel, W., Poremba, K., Tillmann, U., 1999. The importance of sediments in the transformation and turnover of nutrients and organic matter in the Wadden Sea and German Bight. Dtsch. Hydrogr. Zeitschrift 51, 245–266.
Bowles, M.W., Mogollón, J.M., Kasten, S., Zabel, M., Hinrichs, K.U., 2014. Global rates of marine sulfate reduction and implications for sub–sea-floor metabolic activities. Science 344 (6186), 889–891.
Burson, A., Stomp, M., Akil, L., Brussaard, C.P., Huisman, J., 2016. Unbalanced reduction of nutrient loads has created an offshore gradient from phosphorus to nitrogen limitation in the North Sea. Limnol. Oceanogr. 61, 869–888.
Canfield, D.E., 1989. Reactive iron in marine sediments. Geochim. Cosmochim. Acta 53, 619–632.
Canfield, D.E., Jørgensen, B.B., Fossing, H., Glud, R., Gundersen, J., Ramsing, N.B., Thamdrup, B., Hansen, J.W., Nielsen, L.P., Hall, P.O.J., 1993. Pathways of organic carbon oxidation in three continental margin sediments. Mar. Geol. 113, 27–40.
Chambers, R.M., Odum, W.E., 1990. Porewater oxidation, dissolved phosphate and the iron curtain. Biogeochemistry 10 (1), 37–52.
Cline, J.D., 1969. Spectrophotometric determination of hydrogen sulfide in natural waters 1. Limnol. Oceanogr. 14, 454–458.
Coleman, M.L., Hedrick, D.B., Lovley, D.R., White, D.C., Pye, K., 1993. Reduction of Fe(III) in sediments by sulphate-reducing bacteria. Nature 361, 436–438.
Cook, P.L., Wenzhöfer, F., Glud, R.N., Janssen, F., Huettel, M., 2007. Benthic solute exchange and carbon mineralization in two shallow subtidal sandy sediments: effect of advective pore-water exchange. Limnol. Oceanogr. 52, 1943–1963.
Dellwig, O., Leipe, T., März, C., Glockzin, M., Pollehne, F., Schnetger, B., Yakushev, E.V., Böttcher, M.E., Brumsack, H.-J., 2010. A new particulate Mn–Fe–P-shuttle at the redoxcline of anoxic basins. Geochim. Cosmochim. Acta 74, 7100–7115.
Egger, M., Jilbert, T., Behrends, T., Rivard, C., Slomp, C.P., 2015. Vivianite is a major sink for phosphorus in methanogenic coastal surface sediments. Geochim. Cosmochim. Acta 169, 217–235.
Fabiano, M., Danovaro, R., Fraschetti, S., 1995. A three-year time series of elemental and biochemical composition of organic matter in subtidal sandy sediments of the Ligurian Sea (northwestern Mediterranean). Cont. Shelf Res. 15, 1453–1469.
Filippelli, G.M., Delaney, M.L., 1996. Phosphorus geochemistry of equatorial Pacific sediments. Geochim. Cosmochim. Acta 60, 1479–1495.
Gao, H., Matyka, M., Liu, B., Khalili, A., Kostka, J.E., Collins, G., Jansen, S., Holtappels, M., Jensen, M.M., Badewien, T.H., 2012. Intensive and extensive nitrogen loss from intertidal permeable sediments of the Wadden Sea. Limnol. Oceanogr. 57, 185–198.
Gao, L., Li, R., Liang, Z., Yan, C., Zhu, A., Li, S., Yang, Z., He, H., Gan, H., Chen, J., 2020. Remobilization mechanism and release characteristics of phosphorus in saline sediments

from the Pearl River Estuary (PRE), South China, based on high-resolution measurements. Sci. Total Environ. 703, 134411.
Gorski, C.A., Scherer, M.M., 2011. Fe2+ sorption at the Fe oxide-water interface: a revised conceptual framework. Aquatic Redox Chemistry. ACS Publications, pp. 315–343.
Haese, R.R., 2006. The biogeochemistry of iron. Marine Geochemistry. Springer, pp. 241–270.
Hall, S.J., 2002. The continental shelf benthic ecosystem: current status, agents for change and future prospects. Environ. Conserv. 29, 350–374.
Henkel, S., Kasten, S., Hartmann, J.F., Silva-Busso, A., Staubwasser, M., 2018. Iron cycling and stable Fe isotope fractionation in Antarctic shelf sediments,King George Island. Geochim. Cosmochim. Acta 237, 320–338.
Hoffmann, T.D., Reeksting, B.J., Gebhard, S., 2021. Bacteria-induced mineral precipitation: a mechanistic review. Microbiology 167.
Huettel, M., Ziebis, W., Forster, S., Luther, G.W., 1998. Advective transport affecting metal and nutrient distributions and interfacial fluxes in permeable sediments. Geochim. Cosmochim. Acta 62, 613–631.
Huettel, M., Berg, P., Kostka, J.E., 2014. Benthic exchange and biogeochemical cycling in permeable sediments. Annu. Rev. Mar. Sci. 6, 23–51.
Jensen, H.S., Mortensen, P., Andersen, F., Rasmussen, E., Jensen, A., 1995. Phosphorus cycling in a coastal marine sediment, Aarhus Bay, Denmark. Limnol. Oceanogr. 40, 908–917.
Jørgensen, B.B., 2006. Bacteria and marine biogeochemistry. Marine Geochemistry. Springer, pp. 169–206.
Jørgensen, B.B., Kasten, S., 2006. Sulfur cycling and methane oxidation. Marine Geochemistry. Springer, pp. 271–309.
Kamran, A., Schneider, D., Roddatis, V., Thiel, V., Hoppert, M., 2020. Formation of siderite in microbial microcosms derived from a marine sediment. Geomicrobiol. J. 37, 475–485.
Kappler, A., Bryce, C., Mansor, M., Lueder, U., Byrne, J.M., Swanner, E.D., 2021. An evolving view on biogeochemical cycling of iron. Nat. Rev. Microbiol. 19, 360–374.
Kasten, S., Freudenthal, T., Gingele, F.X., Schulz, H.D., 1998. Simultaneous formation of iron-rich layers at different redox boundaries in sediments of the Amazon deep-sea fan. Geochim. Cosmochim. Acta 62, 2253–2264.
Kazmierczak, J., Postma, D., Müller, S., Jessen, S., Nilsson, B., Czekaj, J., Engesgaard, P., 2020. Groundwater-controlled phosphorus release and transport from sandy aquifer into lake. Limnol. Oceanogr. 65, 2188–2204.
Keil, R.G., Montluçon, D.B., Prahl, F.G., Hedges, J.I., 1994. Sorptive preservation of labile organic matter in marine sediments. Nature 370, 549–552.
Kraal, P., Burton, E.D., Rose, A.L., Kocar, B.D., Lockhart, R.S., Grice, K., Bush, R.T., Tan, E., Webb, S.M., 2015. Sedimentary iron–phosphorus cycling under contrasting redox conditions in a eutrophic estuary. Chem. Geol. 392, 19–31.
Kristensen, E., Ahmed, S.I., Devol, A.H., 1995. Aerobic and anaerobic decomposition of organic matter in marine sediment: which is fastest? Limnol. Oceanogr. 40, 1430–1437.
Kristiansen, K., Kristensen, E., Jensen, E., 2002. The influence of water column hypoxia on the behaviour of manganese and iron in sandy coastal marine sediment. Estuar. Coast. Shelf Sci. 55, 645–654.
Krom, M.D., Berner, R.A., 1981. The diagenesis of phosphorus in a nearshore marine sediment. Geochim. Cosmochim. Acta 45 (2), 207–216.
Küster-Heins, K., Steinmetz, E., De Lange, G.J., Zabel, M., 2010. Phosphorus cycling in marine sediments from the continental margin off Namibia. Mar. Geol. 274, 95–106.
März, C., Poulton, S.W., Beckmann, B., Küster, K., Wagner, T., Kasten, S., 2008. Redox sensitivity of P cycling during marine black shale formation: dynamics of sulfidic and anoxic, non-sulfidic bottom waters. Geochim. Cosmochim. Acta 72, 3703–3717.
März, C., Riedinger, N., Sena, C., Kasten, S., 2018. Phosphorus dynamics around the sulphate-methane transition in continental margin sediments: authigenic apatite and Fe (II) phosphates. Mar. Geol. 404, 84–96.
Michaud, A.B., Laufer, K., Findlay, A., Pellerin, A., Antler, G., Turchyn, A.V., Røy, H., Wehrmann, L.M., Jørgensen, B.B., 2020. Glacial influence on the iron and sulfur cycles in Arctic fjord sediments (Svalbard). Geochim. Cosmochim. Acta 280, 423–440.
Pan, F., Guo, Z., Cai, Y., Liu, H., Wu, J., Fu, Y., Wang, B., Gao, A., 2019. Kinetic exchange of remobilized phosphorus related to phosphorus-iron-sulfur biogeochemical coupling in coastal sediment. Water Resour. Res. 55, 10494–10517.
Peiffer, S., Kappler, A., Haderlein, S., Schmidt, C., Byrne, J., Kleindienst, S., Vogt, C., Richnow, H., Obst, M., Angenent, L., 2021. A biogeochemical–hydrological framework for the role of redox-active compounds in aquatic systems. Nat. Geosci. 14, 264–272.
Precht, E., Huettel, M., 2004. Rapid wave-driven advective pore water exchange in a permeable coastal sediment. J. Sea Res. 51, 93–107.
Precht, E., Franke, U., Polerecky, L., Huettel, M., 2004. Oxygen dynamics in permeable sediments with wave-driven pore water exchange. Limnol. Oceanogr. 49, 693–705.
Rao, A.M., McCarthy, M.J., Gardner, W.S., Jahnke, R.A., 2007. Respiration and denitrification in permeable continental shelf deposits on the South Atlantic Bight: rates of carbon and nitrogen cycling from sediment column experiments. Cont. Shelf Res. 27, 1801–1819.
Reed, D.C., Slomp, C.P., Gustafsson, B.G., 2011. Sedimentary phosphorus dynamics and the evolution of bottom-water hypoxia: a coupled benthic–pelagic model of a coastal system. Limnol. Oceanogr. 56, 1075–1092.
Rickard, D., Luther, G.W., 2007. Chemistry of iron sulfides. Chem. Rev. 107, 514–562.
Riedinger, N., Pfeifer, K., Kasten, S., Garming, J.F.L., Vogt, C., Hensen, C., 2005. Diagenetic alteration of magnetic signals by anaerobic oxidation of methane related to a change in sedimentation rate. Geochim. Cosmochim. Acta 69, 4117–4126.
Riedinger, N., Brunner, B., Formolo, M.J., Solomon, E., Kasten, S., Strasser, M., Ferdelman, T.G., 2010. Oxidative sulfur cycling in the deep biosphere of the Nankai Trough, Japan. Geology 38, 851–854.
Riedinger, N., Brunner, B., Krastel, S., Arnold, G.L., Wehrmann, L.M., Formolo, M.J., Beck, A., Bates, S.M., Henkel, S., Kasten, S., 2017. Sulfur cycling in an iron oxide-dominated, dynamic marine depositional system: the Argentine continental margin. Front. Earth Sci. 5, 33.
Roden, E.E., Edmonds, J.W., 1997. Phosphate mobilization in iron-rich anaerobic sediments: microbial Fe (III) oxide reduction versus iron-sulfide formation. Arch. Hydrobiol. 347–378.
Rozan, T.F., Taillefert, M., Trouwborst, R.E., Glazer, B.T., Ma, S., Herszage, J., Valdes, L.M., Price, K.S., Luther III, G.W., 2002. Iron-sulfur-phosphorus cycling in the sediments of a shallow coastal bay: implications for sediment nutrient release and benthic macroalgal blooms. Limnol. Oceanogr. 47, 1346–1354.
Rusch, A., Huettel, M., Wild, C., Reimers, C.E., 2006. Benthic oxygen consumption and organic matter turnover in organic-poor, permeable shelf sands. Aquat. Geochem. 12, 1–19.
Ruttenberg, K.C., 1992. Development of a sequential extraction method for different forms of phosphorus in marine sediments. Limnol. Oceanogr. 37, 1460–1482.
Santos, I.R., Eyre, B.D., Huettel, M., 2012. The driving forces of porewater and groundwater flow in permeable coastal sediments: a review. Estuar. Coast. Shelf Sci. 98, 1–15.
Slomp, C., Van der Gaast, S., Van Raaphorst, W., 1996. Phosphorus binding by poorly crystalline iron oxides in North Sea sediments. Mar. Chem. 52, 55–73.
Slomp, C., Malschaert, J., Lohse, L., Van Raaphorst, W., 1997. Iron and manganese cycling in different sedimentary environments on the North Sea continental margin. Cont. Shelf Res. 17, 1083–1117.
Smith, L., Watzin, M.C., Druschel, G., 2011. Relating sediment phosphorus mobility to seasonal and diel redox fluctuations at the sediment–water interface in a eutrophic freshwater lake. Limnol. Oceanogr. 56, 2251–2264.
Stookey, L.L., 1970. Ferrozine - a new spectrophotometric reagent for iron. Anal. Chem. 42, 779–781.
Thamdrup, B., Fossing, H., Jørgensen, B.B., 1994. Manganese, iron and sulfur cycling in a coastal marine sediment, Aarhus Bay,Denmark. Geochim. Cosmochim. Acta 58, 5115–5129.
Van Cappellen, P., Wang, Y., 1996. Cycling of iron and manganese in surface sediments; a general theory for the coupled transport and reaction of carbon, oxygen, nitrogen, sulfur, iron, and manganese. Am. J. Sci. 296, 197–243.
Van De Velde, S., Meysman, F.J., 2016. The influence of bioturbation on iron and Sulphur cycling in marine sediments: a model analysis. Aquat. Geochem. 22 (5), 469–504.
Viollier, E., Inglett, P., Hunter, K., Roychoudhury, A., Van Cappellen, P., 2000. The ferrozine method revisited: Fe (II)/Fe (III) determination in natural waters. Appl. Geochem. 15, 785–790.
Voelz, J.L., Johnson, N.W., Chun, C.L., Arnold, W.A., Penn, R.L., 2019. Quantitative dissolution of environmentally accessible iron residing in iron-rich minerals: a review. ACS EarthSpace Chem. 3, 1371–1392.
Volkenborn, N., Polerecky, L., Wethey, D.S., Woodin, S., 2010. Oscillatory porewater bioadvection in marine sediments induced by hydraulic activities of Arenicola marina. Limnol. Oceanogr. 55, 1231–1247.
Werner, U., Billerbeck, M., Polerecky, L., Franke, U., Huettel, M., Van Beusekom, J.E., De Beer, D., 2006. Spatial and temporal patterns of mineralization rates and oxygen distribution in a permeable intertidal sand flat (Sylt, Germany). Limnol. Oceanogr. 51, 2549–2563.
Weston, N.B., Porubsky, W.P., Samarkin, V.A., Erickson, M., Macavoy, S.E., Joye, S.B., 2006. Porewater stoichiometry of terminal metabolic products, sulfate, and dissolved organic carbon and nitrogen in estuarine intertidal creek-bank sediments. Biogeochemistry 77, 375–408.
Wu, S., Zhao, Y., Chen, Y., Dong, X., Wang, M., Wang, G., 2019. Sulfur cycling in freshwater sediments: a cryptic driving force of iron deposition and phosphorus mobilization. Sci. Total Environ. 657, 1294–1303.
Wunder, L.C., Aromokeye, D.A., Yin, X., Richter-Heitmann, T., Willis-Poratti, G., Schnakenberg, A., Otersen, C., Dohrmann, I., Römer, M., Bohrmann, G., Kasten, S., Friedrich, M.W., 2021. Iron and sulfate reduction structure microbial communities in (sub-)Antarctic sediments. ISME J. 15, 3587–3604.
Zeng, Z., Tice, M., 2014. Promotion and nucleation of carbonate precipitation during microbial iron reduction. Geobiology 12, 362–371.
Zhao, Y., Zhang, Z., Wang, G., Li, X., Ma, J., Chen, S., Deng, H., Annalisa, O.-H., 2019. High sulfide production induced by algae decomposition and its potential stimulation to phosphorus mobility in sediment. Sci. Total Environ. 650, 163–172.